ARTICLE

Mechanisms for overcharging of carbon electrodes in lithium-ion/sodium-ion batteries analysed by *operando* solid-state NMR

Received 00th January 20xx,
Accepted 00th January 20xx

DOI: 10.1039/x0xx00000x

Kazuma Gotoh,*[ab] Tomu Yamakami, [a] Ishin Nishimura, [a] Hina Kometani, [a] Hideka Ando, [a] Kenjiro Hashi, [c] Tadashi Shimizu, [c] and Hiroyuki Ishida [a]

A precise understanding of the mechanism for metal (Li and Na) plating on negative electrodes that occurs with overcharging is critical to managing the safety of lithium- and sodium-ion batteries. In this work, an in-depth investigation of the overlithiation/oversodiation and subsequent delithiation/desodiation of graphite and hard carbon electrodes in the first cycle was conducted using *operando* ^{7}Li/^{23}Na solid-state NMR. In the ^{7}Li NMR spectra of half cells of carbon electrodes and metal counter electrodes, three types of signals corresponding to Li dendrites that formed on the surface of graphite, hard carbon, and the counter electrode were distinguished from the signal of Li metal foil of the counter electrode by applying an appropriate orientation of the testing cell. For graphite overlithiation, the deposition of Li dendrites started immediately or soon after the minimum electric potential in the lithiation curve. In contrast, the deposition of Li dendrites in hard carbon started after the end of quasimetallic lithium formation for overlithiation at rates below 3.0C. Similar behaviour was also observed for the oversodiation of hard carbon. The formation of quasimetallic Li or Na in the pores of hard carbon serves as a buffer for the metal plating that occurs with overcharging of the batteries. Furthermore, some of the deposited Li/Na dendrites contribute to reversible capacities. A mechanism for the inhomogeneous disappearance of quasimetallic Li during delithiation of hard carbon is also proposed.

Introduction

The market for secondary batteries such as lithium-ion batteries (LIBs) has been growing steadily for the last 20 years because of the increasing demand for energy storage devices for products such as smart phones and electric vehicles (EVs).[1,2] In particular, popularization of large-size batteries for vehicles and infrastructures is expected in the next decade, which will require a very large number of cells and an enormous amount of raw materials. Hence, not only LIBs but also novel secondary batteries such as sodium-ion batteries (NIBs) are receiving attention as potential cost-effective systems.[3,4]

With the expansion of the LIB market, the number of fire accidents related to LIBs is also increasing.[5] Most of these accidents have occurred during battery charging. Contamination of the electrode materials with conductive impurities is one of the problems that lead to fires. Overcharging of batteries by inappropriate charging processes is also a cause of accidents. In the latter case, overcharging of a LIB using a broken or an unauthorized charger can lead to the formation of dendritic lithium on the surface of the negative electrode material. The dendritic lithium grows and penetrates the separator in the battery, finally causing a short circuit.[6] Therefore, investigation of the dendritic lithium (Li dendrites) is critical to managing and improving the safety of LIBs.

The formation of Li dendrites on the surface of carbon negative electrodes in LIBs was observed by Su et al. using scanning electron microscopy (SEM) and spectroscopic methods including *ex situ* solid-state nuclear magnetic resonance (SSNMR).[7] In the overcharged states of the graphite and hard carbon electrodes in half cells using lithium metal as the counter electrode, Li dendrites appeared after the minimum electric potentials were reached in the overlithiation (overdischarge) curves (−0.03 and −0.05 V for graphite and hard carbon, respectively). Li dendrites did not appear before this minimum potential was reached even though the potential was below 0 V. The differences in the formation mechanisms of Li dendrites on graphite and hard carbon were also revealed. Lithium nucleation and the initial growth of Li dendrites occurred inhomogeneously on the graphite surfaces during the overlithiation process, whereas lithium nucleation and initial growth occurred inside nanopores and generated dendrites with smooth, clean surfaces during the overlithiation process for hard carbon. However, because the previous experiments were performed *ex situ*, the precise onset times of dendrite formation in the overlithiation curves could not be determined. From the viewpoint of battery safety, detailed investigation of the overlithiation process and dendrite deposition is crucial.

[a] *Graduate School of Natural Science & Technology, Okayama University, 3-1-1 Tsushima-naka, Okayama 700-8530, Japan. E-mail: kgotoh@okayama-u.ac.jp*
[b] *Element Strategy Initiative for Catalysts and Batteries (ESICB), Kyoto University, Nishikyo-ku, Kyoto 615-8245, Japan.*
[c] *National Institute for Materials Science, Tsukuba, Ibaraki 305-0003, Japan.*
† Electronic Supplementary Information (ESI) available: [NMR sample setting, supplemental NMR spectra and peak fittings]. See DOI: 10.1039/x0xx00000x

Operando investigation of the battery is needed to observe the transition of the state of a battery in real time.

Several analytical methods with *in situ* or *operando* measurements can be used to investigate the state of batteries as they allow the non-equilibrium state of the battery during charging and discharging processes to be accessed.[8-10] One of these methods, *in situ* or *operando* SSNMR of Li and Na nuclei, is also suitable for characterizing the negative electrode in LIBs and NIBs[11,12] as Li/Na NMR can be used to observe the entire Li or Na nuclei in samples containing nuclei stored in the inner structure of materials, which are not easily observed directly by SEM or X-ray analyses. For the negative electrode materials of LIBs and NIBs, the behaviour of Li[13-20] and Na[21] in carbon electrodes and metal electrodes[22-28] have been observed using *in situ* or *operando* NMR. Very recently, *in situ* magic angle spinning (MAS) NMR was also realized.[29] In the current study, we observed the overlithiation processes of graphite and hard carbon electrodes using *operando* ^{7}Li NMR. To observe the state of the Li dendrite on the surface of negative electrodes using *operando* ^{7}Li NMR, analysis of full-cell samples consisting of negative electrodes (carbon) and counter positive electrodes (Li metal oxides) is easier than analysis of half-cell samples consisting of a negative electrode and counter Li metal electrode because the signal of the Li metal electrode does not overlap with the peaks of Li dendrites. However, the electric potential of the negative electrode in bipolar full cells cannot be detected accurately. Therefore, half cells consisting of a carbon electrode and a Li metal electrode were used in the current study. The assembled half cells were analysed continuously during lithiation and following overlithiation.

Our group observed the overcharged states of graphite and hard carbon electrodes in LIB (full cells) using *in situ* ^{7}Li NMR in previous reports.[19, 20, 30] We observed a ''relaxation effect'' of the negative electrodes after overcharging, that is, a decrease of the signal of Li metal deposited on the negative electrode surface. The effect was observed intensely in the first few hours, and the electrodes reached an equilibrium state after 8–15 h.[19] Thus, it is also important to evaluate the behaviour of the Li in the negative electrodes after overlithiation in the overcharged state. In the present study, we also observed the state of electrodes during the delithiation process after the first overlithiation operation. In addition, the mechanism of sodiation and oversodiation were investigated using half cells consisting of hard carbon and Na metal using *operando* ^{23}Na NMR and *ex situ* ^{23}Na NMR analyses.

Experimental

Preparation of cells for *operando* NMR

Cylindrical sample cells for *operando* NMR measurement were prepared using a polyether ether ketone (PEEK) body and a cover (Fig. S1). These cells produce an NMR signal intensity that is 4–5 times stronger than that of our previous *in situ* cells covered by Al-laminate film[19] because rf pulses and NMR signals are not prevented by PEEK. The cells for Li NMR were assembled using working electrodes made of graphite (spherocrystal graphite, Hohsen Co., 340 mAh g^{-1} of Li^{+} capacity) or pitch-based hard carbon (Carbotron P(J), Kureha, 306 mAh g^{-1} of Li^{+} capacity at constant current (CC) lithiation[31]), a separator (glass filter, ADVANTEC), and Li metal foil as the counter electrode. The cells were filled with 1 M $LiPF_6$ in an ethylene carbonate (EC)/diethyl carbonate (DEC) mixture (Battery Grade, Kishida Chemical, 1:1 v/v%) as the electrolyte. For the Na NMR experiments, sucrose-based hard carbon prepared by dehydration at 300 °C and subsequent carbonization at 1600 °C (HC300-1600; analysed in our previous research (369 mAh g^{-1}) [32]) was used because it has the highest sodiation capacity in the sucrose derived hard carbons. The cells were assembled using a working electrode of the hard carbon, and a polyimide binder (DREAM BOND, Industrial Summit Technology), separator (glass filter, ADVANTEC), and Na metal plate as a counter electrode with an electrolyte solution of 1 M $NaPF_6$ EC/DEC (Battery Grade, Kishida Chemical, 1:1 v/v%).

Operando analysis of overcharged state

Operando ^{7}Li NMR experiments were conducted using an Agilent DD2 NMR spectrometer with a 11.7 T superconducting magnet and a homemade probe for *operando* analysis, which had a structure similar to that of our previous *in situ* NMR probe.[19] The cells for analyses were placed in the solenoid coil with the direction of the electrodes in the cells perpendicular to the external static field (Fig. S1). It has been reported that the ^{7}Li chemical shift of the Li metal signal in a flat battery sample shifts depending on the angle between the electrode and external static field because of bulk susceptibility effects.[33, 34] The signals of the Li metal electrode and Li metal dendrite could be distinguished for the same reason.[34, 35] We arranged the cells perpendicular to the static field (Fig. S1), which is the most convenient position to distinguish the counter Li metal electrode and dendritic Li metal on the surface of the carbon or counter electrode because the signal of the Li metal electrode appears at the lowest frequency.[33] *Operando* ^{23}Na NMR spectra were also collected using the same spectrometer and the probe under similar experimental conditions.

The prepared Li cells were galvanostatically lithiated (discharged) at 0.1C–1.0C for the graphite electrodes and 0.3C–4.5C for the hard carbon electrodes, with no lower potential limit setting to induce the overlithiated state (overdischarged state for half cells) of the working electrodes. ^{7}Li NMR spectra of the cells were simultaneously measured during the lithiation and overlithiation process. Every graphite or hard carbon electrode was directly overlithiated with no pre-cycle treatment, except for one graphite electrode, which was pre-cycled once in the range between 2.0 and 0.0 V. The lithiation (discharge) and the acquisition of ^{7}Li NMR spectra were continued until at least 600 mAh g^{-1} for the graphite cells and 1000 mAh g^{-1} for the hard carbon cells. Some of the cells were delithiated (charged) after the overlithiation to observe the process of delithiation from

the carbon electrodes. For the *operando* ^{7}Li NMR spectroscopy, a single pulse sequence with a pulse length of 1.5 μs corresponding to the 45° spin flip was applied. The ^{7}Li NMR signal in 1 M LiCl aqueous solution was adjusted to 0 ppm. A ^{7}Li NMR spectrum was repeatedly collected every 2 min with 60 scans with a recycle delay of 2 s.

The *operando* ^{23}Na NMR spectra were collected under similar conditions as the ^{7}Li NMR spectra using a single pulse sequence with a pulse length of 2.0 μs. Each ^{23}Na NMR spectrum was collected with 500 scans with a recycle delay of 0.5 s, i.e., spectra were repeatedly collected every 250 s. *Ex situ* ^{23}Na MAS NMR spectroscopy was performed using the same apparatus and a MAS probe with a 3.2 mmϕ rotor, as described in our previous reports.[32, 36] Each ^{23}Na MAS NMR spectrum of a sodiated hard carbon sample was collected using a single pulse sequence with a pulse length of 2.0 μs with 2000 scans. 1 M NaCl aqueous solution was used as a standard for the chemical shift (0 ppm).

Results and Discussion

First lithiation in graphite cells

The discharge profile of a graphite electrode at 0.35C without pre-cycling treatment and the corresponding *operando* ^{7}Li NMR spectra are presented in Fig. 1(a)–(d). The electric potential gradually decreased to 0.0 V as lithiation proceeded. Subsequently, the electric potential became negative, which indicates the overlithiated state of the working electrode, and reached a minimum potential (−0.055 V) 189 min after lithiation began. After reaching the minimum, the potential increased slightly and then remained almost constant (−0.051 V) (Fig. 1(a)). In the corresponding *operando* ^{7}Li NMR spectra (Fig. 1(b)–(d)), signals of Li ion in electrolyte solution near −1 ppm (ES) and of Li metal of the counter electrode (Li CE) (240–270 ppm) were observed in every spectrum. Additionally, signals of Li in the graphite layers (LiC_6, LiC_{12}) at approximately 38 ppm and of dendritic Li metal (Li de) at approximately 258 ppm appeared as a new peak and a shoulder structure of Li CE, respectively, during lithiation and overlithiation.

As precise estimation of the onset time of Li dendrite deposition directly from Fig. 1(b)(c) was difficult, the Li metal signals were fit with three Gaussian curves. Two curves (with

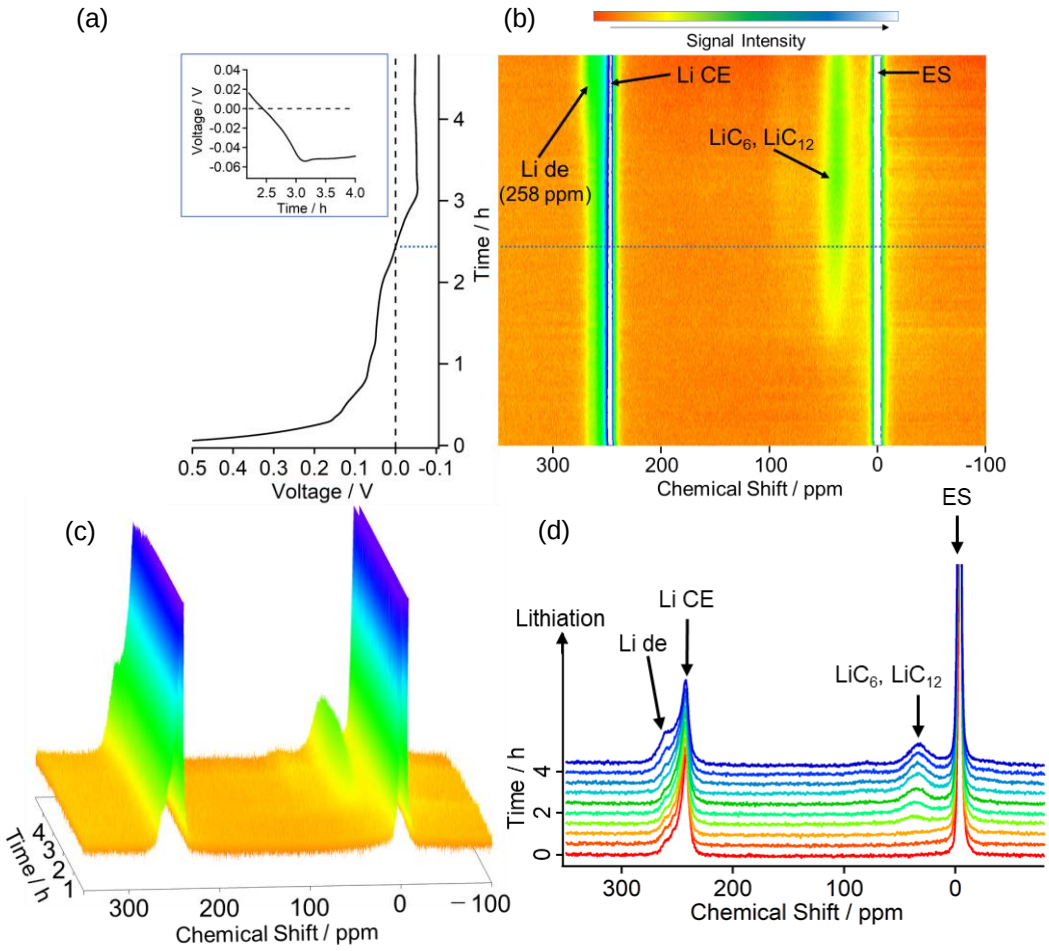

Fig. 1 Discharge (lithiation) profile of graphite electrode at 0.35C without pre-cycling treatment (a) and corresponding *operando* ^{7}Li NMR spectra (b). (c) 3D view of the spectra in (b). The 1D spectra arranged in (d) were extracted from the spectra in (b).

peaks at 242 and 248 ppm) were expediently attributed to the Li CE signal (Fig. S2(a)), which have constant signal intensity and do not change with lithiation/delithiation, and one curve was for Li de at 258 ppm, which increases with the overlithiation process. The signal intensity (area) of Li de increased proportionally with time (Fig. S2(b)); hence, we estimated the time when the intensity of Li de was zero by extrapolating the fitting line. The estimated onset time of Li dendrite deposition was determined to be 194 min, which is 5 min later than the time at which the minimum electric potential appeared (Table 1).

The discharging profile and corresponding *operando* ^{7}Li NMR spectra for similar experiments with a lower lithiation rate (0.10C) are presented in Fig. 2(a) and (b), respectively. A potential minimum in the overlithiation state under 0.0 V and deposition of Li dendrites were also observed. The observed times for the minimum electric potential and the estimated starting times of Li dendrite deposition of graphite electrodes are summarized in Table 1. The deposition of Li dendrites in each experiment started immediately or soon after the minimum potential appeared in the lithiation curve. These results strongly suggest that the state of lithium crammed into graphite electrodes between 0.0 V and the potential minimum is an instable phase before crystallization. Because graphite electrode is fully intercalated as LiC_6 at that state, additional Li atoms locate on the surface (edge sites or defect sites) of graphite particles. Some Li atoms on the surface may aggregate and form sub-nanometre size clusters or particles, but it is too small to have the property of Li metal at that time. The formation of Li metal crystal requires additional electric potential of approximately −0.033 V, which is the minimum potential of the overlithiation curve.

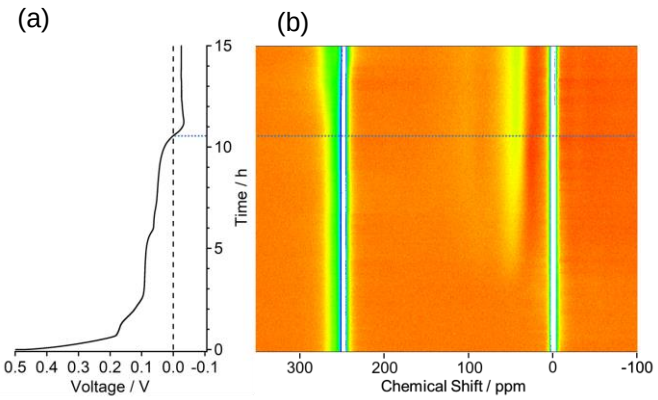

Fig. 2 Discharge (lithiation) profile of graphite electrode at 0.10C without pre-cycling treatment (a) and corresponding *operando* ^{7}Li NMR spectra (b).

Experiments using discharging rates of 1C or larger in the first lithiation resulted in considerable decrease of the capacities of the cells. Nevertheless, the behaviours of the overlithiation profile and dendrite deposition were similar to those observed for the slower lithiation experiments shown in Figs. 1 and 2. The detailed experimental results for lithiation at approximately 1C are presented in the ESI (Fig. S3).

Table 1 Lithiation (discharge) rate, time corresponding to potential of 0.0 V, time corresponding to minimum potential, and estimated onset time of Li dendrite deposition of graphite electrode

lithiation rate	time at potential of 0.0 V (min)	time at minimum potential (min)	onset time of Li dendrite deposition (min)
0.35C	146	189	194
0.10C	633	674	703

Delithiation after overlithiation in graphite cells

The charging profile (delithiation curve) and corresponding NMR spectra following the lithiation at 0.35C of the graphite cell (Fig. 1) are presented in Fig. 3(a) and (b), respectively. The signal for Li dendrites at 258 ppm decreased gradually with delithiation during the first 2 h (from 4.8 to 6.8 h in Fig. 3); however, the dendrite signal increased again following the decrease. The peak shift of the regrown dendrite signal was 266 ppm, which is slightly higher than the first dendrite signal. The former peak, which decreased at the start of delithiation, is the Li dendrite signal formed on the surface of the graphite electrode, and the latter regrown peak is attributed to the Li dendrites formed on the surface of the Li metal counter electrode. The assignment can be explained by the effect of bulk susceptibility from the Li metal foil to the dendrite, which was observed as a shift of the LiC_6 signal to higher frequency by the bulk susceptibility of a $LiMn_2O4$ (LMO) electrode in ref.[19]

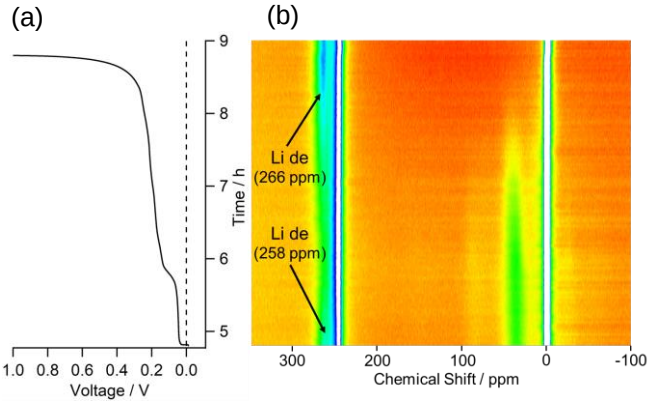

Fig. 3 Charge (delithiation) profile of graphite electrode at 0.35C after overlithiation shown in Fig. 1. (a) and corresponding *operando* ^{7}Li NMR spectra (b).

The second cycle of overlithiation and delithiation profiles of the graphite electrode and corresponding NMR spectra at 0.3C after the first lithiation/delithiation cycle at 0.1C between 2.0~0.0 V are displayed in Fig. S4. Although the capacity of the cell decreased considerably in the first cycle, the deposition of

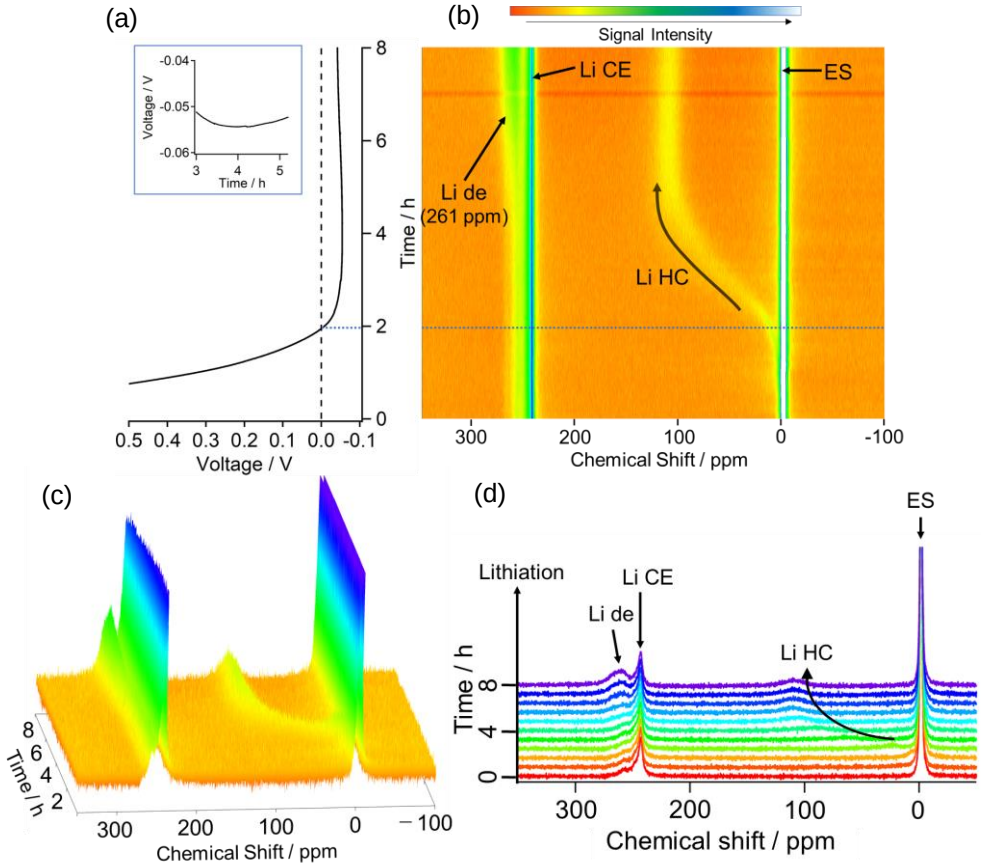

Fig. 4 Discharge (lithiation) profile of hard carbon electrode at 0.4C without pre-cycling treatment (a) and corresponding *operando* ^{7}Li NMR spectra (b). (c) 3D view of spectra in (b). The 1D spectra arranged in (d) were extracted from the spectra in (b).

Li de on graphite at 258 ppm during overlithiation and the signal of Li de on the counter electrode during delithiation at 266 ppm were similarly observed. Despite the similar metal states of lithium, the signals of the Li metal electrode, dendrite on graphite, and dendrite on the counter electrodes were clearly distinguished by the *operando* ^{7}Li NMR.

First lithiation in hard carbon cells

The discharging profile of the hard carbon electrode at 0.4C without pre-cycling treatment and the corresponding ^{7}Li NMR spectra are presented in Fig. 4 (a)–(d). The potential also gradually decreased and fell below 0.0 V with lithiation, which are similar to a previous report.[7] The potential reached a minimum (−0.054 V) after 237 min. After reaching the minimum, the potential remained almost constant (−0.050 V) (Fig. 4(a)). In the corresponding ^{7}Li NMR spectra (Fig. 4(b)–(d)), not only signals of Li ion in the electrolyte solution at −2 ppm (ES) and of Li metal of the counter electrode (Li CE) (240–270 ppm) but also signals of Li in hard carbon at 5~110 ppm (Li HC) and Li dendrite (Li de) at approximately 262 ppm were observed with lithiation and overlithiation. The signal of Li HC gradually shifted from 5 to 110 ppm because of the formation of quasimetallic lithium clusters in the pores of hard carbon.[31]

The onset time of Li dendrite (Li de) deposition, which was also derived by extrapolating the fitting line for peak areas using the same procedure as that used for graphite electrodes (Fig. S5), was 301 min. This time is 64 min after the time of the potential minimum in the lithiation curve. The shift of Li HC signals proceeded after the potential minimum and before lithium deposition. Interestingly, the lithium deposition started immediately after the end of the shift of the HC signal to 110 ppm (Table 2), whereas the formation of quasimetallic clusters has been mainly observed during potentiostatic (constant voltage) lithiation processes (CV) in CC–CV charging.[31] In the current study, we clearly revealed that the formation of

Table 2 Lithiation (discharge) rates, times corresponding to potential of 0.0 V, times corresponding to minimum potential, times corresponding to end of Li-cluster formation, and estimated onset times of Li dendrite deposition of hard carbon electrodes.

lithiation rate	time at potential of 0.0 V (min)	time at minimum potential (min)	end of quasi-metallic cluster formation (min)	onset time of Li dendrite deposition (min)
0.4C	118	237	280	301
0.7C	84	162	206	209
3.0C	6.3	15.2	54.0	19.0
4.5C	3.6	17.5	23.0	18.6

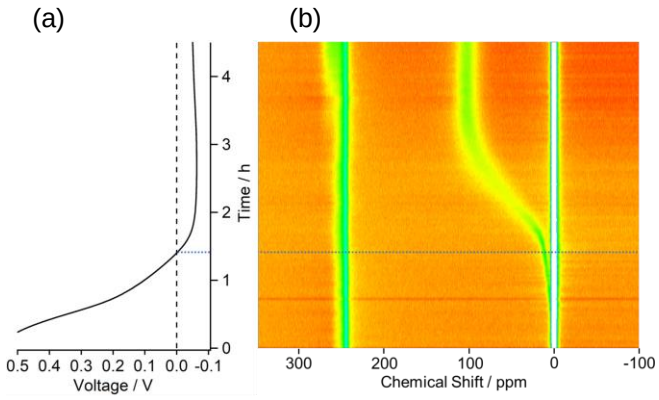

Fig. 5 Discharge (lithiation) profile of hard carbon electrode at 0.7C without pre-cycling treatment (a) and corresponding *operando* ^{7}Li NMR spectra (b).

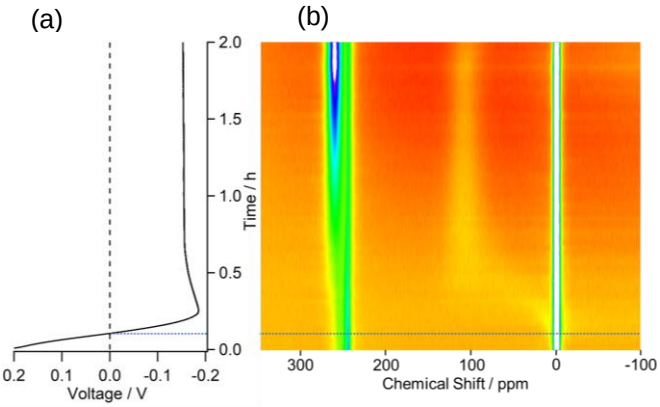

Fig. 6 Discharge (lithiation) profile of hard carbon electrode at 3.0C without pre-cycling treatment (a) and corresponding *operando* ^{7}Li NMR spectra (b).

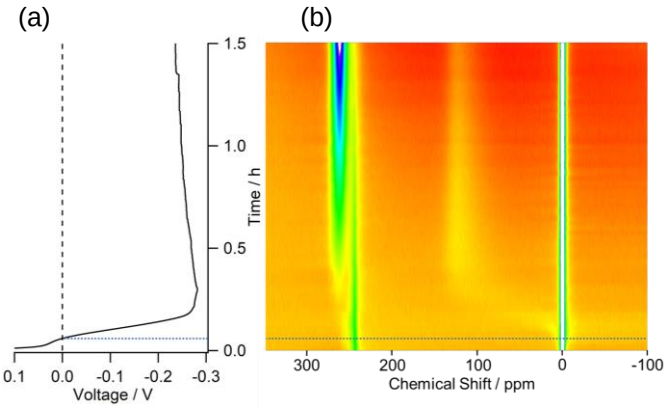

Fig. 7 Discharge (lithiation) profile of hard carbon electrode at 4.5C without pre-cycling treatment (a) and corresponding *operando* ^{7}Li NMR spectra (b).

quasimetallic Li clusters occurs before dendrite deposition in HC electrodes even for overlithiation processes at 0.4C.

The results of similar experiments at faster lithiation rate (0.7C, 3.0C, and 4.5C) are presented in Figs. 5~7. The observed times at 0.0 V, the potential minima, the end of quasimetallic Li cluster formations, and the onsets of dendrite deposition are also summarized in Table 2. In the lithiation and overlithiation processes of hard carbon electrodes at lithiation rates of 0.4C and 0.7C, the formation of quasimetallic Li clusters started near the electric potential of 0.0 V. Its formation continued until the minimum potential of approximately −0.05 V and was complete before the lithium dendrite deposition. Finally, the dendrite deposition started immediately after the end of quasimetallic cluster formation. This result strongly suggests that the formation of quasimetallic clusters can serve as a buffer for the deposition of Li dendrites during overcharging of the batteries. A similar experiment at a lithiation rate of 1.5C also demonstrated the same process, although a potential minimum was not clearly observed in the lithiation profile (Fig. S6). In contrast, for fast overlithiation at 3.0C and 4.5C, Li dendrite deposition started before the end of quasimetallic cluster formation (Table 2). The onset of Li dendrite deposition in 3.0C and 4.5C lithiation (approximately 19 min) occurred immediately after the minimum potential was reached (after 15.2 and 17.5 min, respectively). In such cases, the potentials of the minima (–0.19 V at 3.0C and –0.28 V at 4.5C) were evidently lower than –0.05 V. These results suggest that the formation of quasimetallic Li clusters and the growth of Li dendrite proceed simultaneously after the minimum potential is reached. Thus, the buffer effect by quasimetallic clusters is insufficient for very fast overlithiation.

As shown in Fig. 1 and Fig. 4, the peak values of Li de signals on the graphite electrode (258 ppm) and hard carbon electrode (261–262 ppm) were slightly different. This finding clearly demonstrates the different circumstances around Li dendrites in graphite and hard carbon electrodes. Su et al. proposed that the Li plating in graphite electrodes by overlithiation starts from the nucleation of lithium metal on the edge side of graphite particles and includes a large amount of lithium degradation products, whereas nucleation of lithium metal starts inside the carbon structure with minimal side reactions for hard carbon electrodes. As a result, knob-like dendrites and dendrites with a smooth clean surface are observed on graphite and hard carbon by SEM, respectively.[7] The different Knight shifts (258 ppm and 261–262 ppm) observed in our NMR spectra acutely reflect the dendrite morphology.

In the above model proposed by Su et al., the growth of dendrite in hard carbon starts inside the carbon structure. However, the ^{7}Li NMR signal intensities of quasimetallic lithium formed by lithiation (in Figs. 4 and 5) do not decrease after the onset of dendrite formation, which suggests that most of the quasimetallic lithium is not involved in the nucleation of Li dendrites. The nucleation of Li dendrites appears to arise only in the pores adjacent to the surface of hard carbon particles.

Delithiation in hard carbon cell

The charging profile (delithiation curve) and corresponding NMR spectra following the overlithiation at 0.3C of the LiHC cell for 12 h are presented in Fig. 8. The signal of Li de on hard carbon (261 ppm) decreased gradually with delithiation during

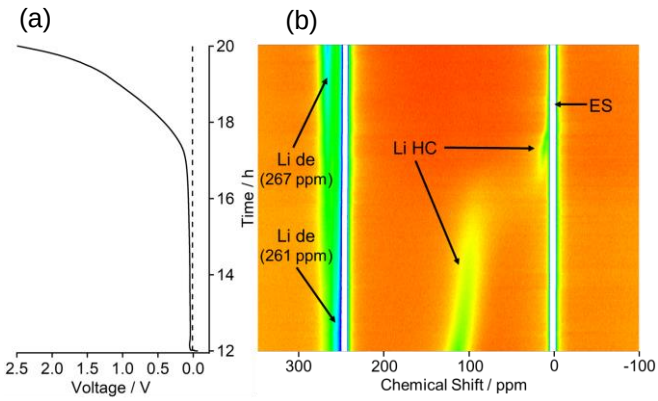

Fig. 8 Charge (delithiation) profile of hard carbon electrode at 0.3C after overlithiation at 0.3C for 12 h (a) and corresponding *operando* ^{7}Li NMR spectra (b).

the first 4 h (from 12 to 16 h in Fig. 8), whereas the signal for Li de on the counter electrode (267 ppm) increased after 17 h. Interestingly, the transition behaviour of the Li HC signal with delithiation was not symmetric with the variation in the lithiation spectra. The signal of the Li HC signal at 110 ppm gradually decreased with a slight shift to lower frequency from 12 to 16 h, then become indistinct and almost disappeared at once. Subsequently, the signal reappeared at approximately 15 ppm after 16.6 h and was finally incorporated with the ES signal (Fig. 8(b)). The results suggest that the mechanisms of lithium storage and release in hard carbon are different. For lithiation, many quasimetallic lithium clusters in the inner pores of hard carbon grow in a simultaneous manner, which is reflected by the gradual shift from 5 to 110 ppm with no signal broadening. However, removal of lithium clusters from the inner pores may occur inhomogeneously during delithiation. Similar to gas adsorption / desorption for inkbottle type pores, the entrance of some pores of hard carbon might be very narrow. The stored Li atoms in such pores are not easily removed. The size distribution of clusters can cause broadening of the Li HC signal. A scheme of lithiation and delithiation suggested from the NMR results is presented in Fig. 9.

First sodiation and desodiation in hard carbon cells

Discharge (sodiation and oversodiation) and charge (desodiation) profiles of the hard carbon electrode at 0.3C without pre-cycling treatment and the corresponding *operando* ^{23}Na NMR spectra are presented in Fig. 10 (a)–(c). The electric potential of the cell also gradually decreased and fell below 0.0 V with sodiation at 148 min after the onset of sodiation. A minimum potential (−0.056 V) was reached after 264 min. After reaching the minimum, the potential remained almost constant (−0.035 V) (Fig. 10(a)). In the corresponding ^{23}Na NMR spectra (Fig. 10(b) and (c)), signals of Na ion in electrolyte solution (ES; −9 ppm), SEI and Na stored in hard carbon (SEI, Na HC; 5 to −20 ppm), Na metal of the counter electrode (Na CE; 1123 ppm), Na

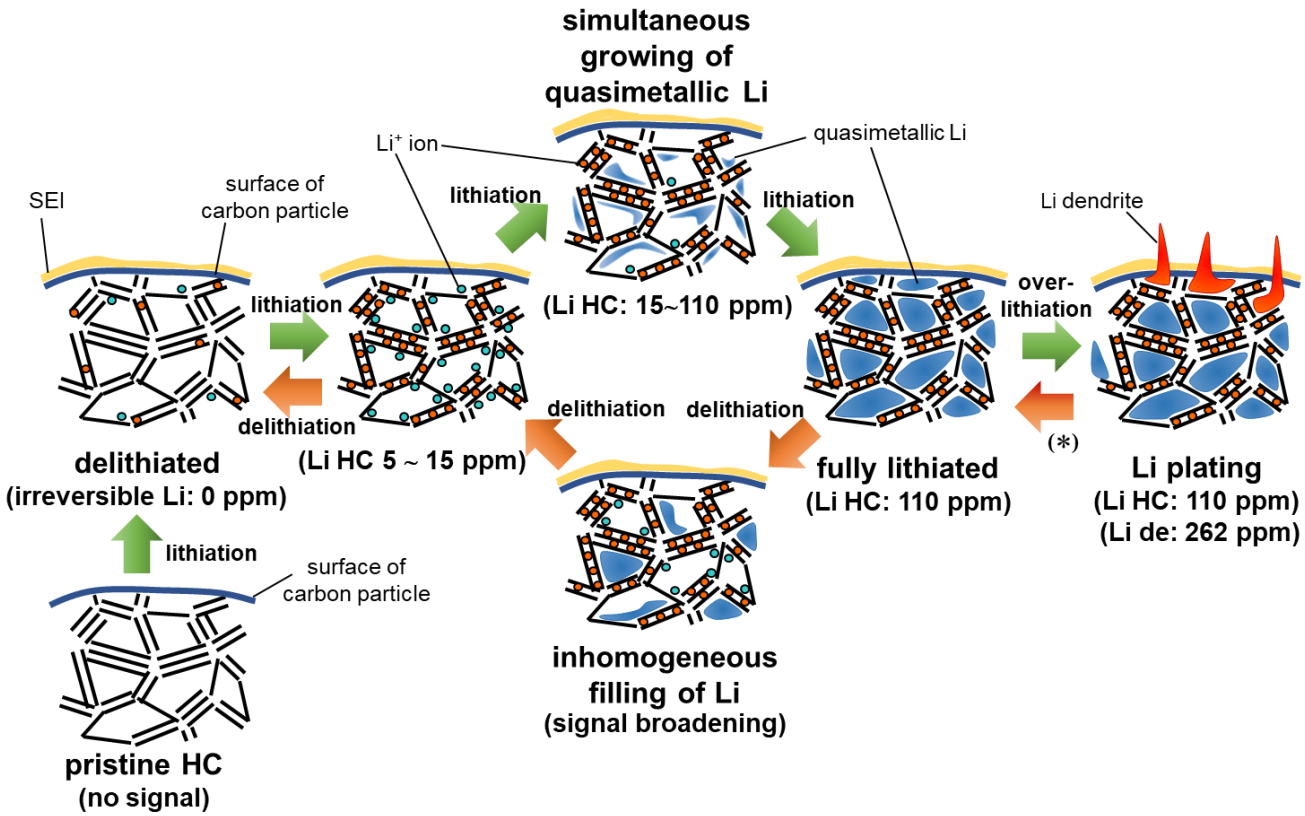

Fig. 9 Mechanism of lithiation and delithiation at hard carbon.
(*) The deposited Li dendrites in the "Li plating" state partially disappear with delithiation but are not completely removed, which is not reflected in the figure.

sodiation time at potential time at minimum onset time of

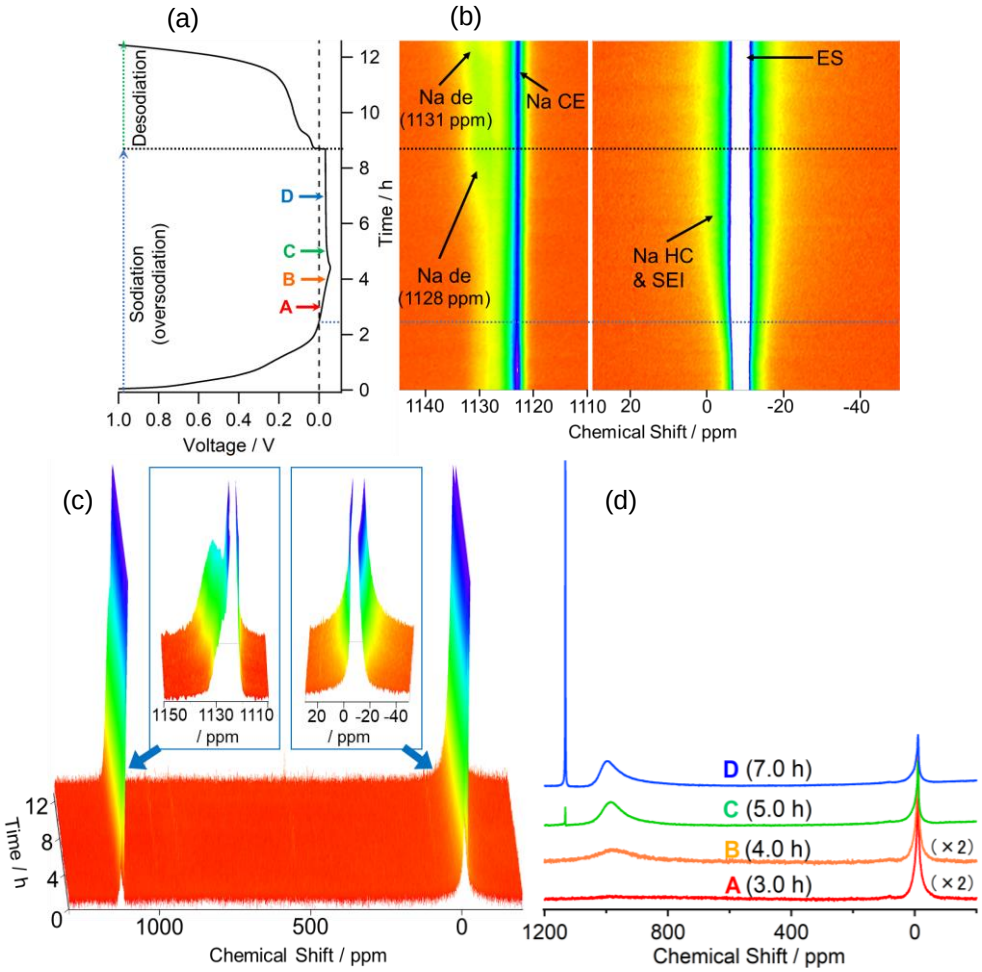

Fig. 10 Discharge (oversodiation) and following charge (desodiation) profiles of hard carbon electrode at 0.3C in the first cycle (a) and the corresponding *operando* ^{23}Na NMR spectra (whole spectra (c) and spectra near −10 and 1125 ppm (b)). (d) ^{23}Na MAS NMR spectra of oversodiated hard carbon samples corresponding to points A, B, C, and D in the sodiation curve in (a).

metal dendrite (Na de) in hard carbon (1128 ppm), and Na de on the counter electrode (1131 ppm) were observed, whereas a signal of quasimetallic sodium, which has been reported at 800–1100 ppm at full sodiation of hard carbon achieved by slow discharging (0.1C)[21, 32], was not observed clearly. The estimated onset time of Na deposition is 294 min, which is 30 min later than the minimum of the potential (Table 3). During the desodiation of the cell, a peak shift of Na de from 1128 to 1131 ppm was observed, which indicates the decreasing of Na dendrites on hard carbon and subsequent growth of the Na dendrites on the counter electrode.

Table 3 Sodiation (discharge) rate, time corresponding to potential of 0.0 V, time corresponding to minimum potential, and estimated onset time of Na dendrite deposition of hard carbon electrode.

sodiation rate	time at potential of 0.0 V (min)	time at minimum potential (min)	onset time of Na dendrite deposition (min)
0.3C	148	264	294

The unappreciable observation of the quasimetallic Na signal in hard carbon in the *operando* NMR spectra is due to the broadening of the signal by the effect of the bulk susceptibility of the counter electrode. The very weak NMR intensity resulting from the small electrode sizes (10 mm × 3.5 mm) and smaller capacity of the tested *operando* cell (82% of the capacity delivered using coin-cell experiments in our previous report) in our experiment might also be influential. To confirm whether the quasimetallic Na was formed during the oversodiation process, some oversodiated hard carbon samples corresponding to points A, B, C, and D in Fig. 10(a) were prepared and measured using *ex situ* ^{23}Na MAS NMR at 12 kHz rotation (Fig. 10(d)). The signal of quasimetallic sodium clearly appeared at points B (4.0 h) and D (7.0 h) in the spectra, whereas the Na de signal was observed at points C (5.0 h) and D (7.0 h). This finding indicates that the formation of

quasimetallic sodium also occurred by oversodiation similar to the case for lithium. The formation started during oversodiation between 0.0 V and the minimum electric potential of the cell.

Deposition and disappearance behaviour of dendrites on graphite and hard carbon electrodes

During the overlithiation of the tested cells by slow discharging, the electric potential of the graphite cells rapidly decreased with clear sharp minima, whereas the potential of the hard carbon cells slowly decreased with broad, obscure minima. The latter behaviour can be explained by the buffer effect arising from the formation of quasimetallic clusters in the inner pores of hard carbon. This effect is also observed for oversodiation to hard carbon (Fig. 10(a)). Experiments of oversodiation at higher discharging rate or overlithiation/oversodiation at different temperatures to estimate the limit of the buffer effect are next important steps, which will provide a better understanding of the behaviour of the batteries.

During the delithiation of the overlithiated graphite cells, the Li dendrite signals clearly decreased (Figs. 3(b) and 8(b)). The results suggest that some of the Li dendrites can work as reversible capacity, which is also gathered from the delithiation capacity in our experiments. The delithiation capacities in Figs. 3(a) and 8(a) were 1.6 and 1.8 times the full lithiation capacity (except for overlithiation under 0.0 V), respectively. This phenomenon was also observed for sodiation; the desodiation capacity in Fig. 10(a) was 1.6 times of initial sodiation capacity (except for oversodiation under 0.0 V). Estimating the amount of reversible Li/Na dendrites on hard carbon is a more complicated issue because of the quasimetallic clusters and will be a topic for future discussion.

Conclusions

In the *operando* ^{7}Li NMR measurements of half cells consisting of a carbon electrode and metal counter electrode, three types of Li dendrite signals (Li de on the surface of graphite, Li de formed on hard carbon, and Li de grown on the counter electrode) could be detected separately from the signal of the counter electrode (Li metal foil) by using an appropriate orientation of the testing cell. The onset times of Li dendrite deposition on the surface of the graphite and hard carbon electrodes were precisely estimated by peak fittings of the signal intensities of Li dendrite components in the NMR spectra. For graphite overlithiation, the deposition of Li dendrites started soon after the appearance of the minimum potential in the lithiation curve. The results suggest that the state of lithium crammed into graphite electrodes between 0.0 V and the potential minimum is an instable phase before crystallization. In overlithiation experiments of hard carbon samples at less than 3.0C, the formation of Li quasimetallic clusters started near the electric potential of 0.0 V and was complete before the lithium dendrite deposition. The dendrite deposition started immediately after the end of quasimetallic cluster formation. During delithiation of hard carbon, shrinkage of Li dendrites and inhomogeneous removal of quasimetallic clusters were observed. The formation of quasimetallic sodium by oversodiation was also discovered using a combination of *operando* and *ex situ* ^{23}Na NMR. The formation and growth of quasimetallic sodium occurred during oversodiation between 0.0 V and the minimum electric potential of the cell.

We revealed that the formation of quasimetallic clusters can serve as a buffer for the deposition of Li and Na dendrites during overcharging of batteries. Closed pores in hard carbon are useful not only for increasing the capacity of the negative electrode but also for serving as a buffer for metal plating that occurs because of accidental overcharging of LIBs and NIBs.

Conflicts of interest

There are no conflicts to declare.

Acknowledgements

This work was supported by JSPS Grants-in-Aid for Scientific Research (KAKENHI) No. 17K06017.

The authors are grateful to Mr. Takashi Oyama and Mr. Ryuji Yokoyama at OTIS Co. Ltd. for designing and fabricating the cells for NMR measurement.

The authors would also like to thank RSC Language Editing service for correction of the English in the manuscript.

References

1 J. M. Tarascon, *Electrochem. Soc. Interface*, 2016, **25**, 79.
2 M. Armand and J. M. Tarascon, *Nature*, 2008, **451**, 652.
3 S. Komaba, W. Murata, T. Ishikawa, N. Yabuuchi, T. Ozeki, T. Nakayama, A. Ogata, K. Gotoh and K. Fujiwara, *Adv. Funct. Mater.*, 2011, **21**, 3859.
4 N. Yabuuchi, K. Kubota, M. Dahbi and S. Komaba, *Chem. Rev.*, 2014, **114**, 11636.
5 L. Kong, C. Li, J. Jiang and M. Pecht, *Energies*, 2018, **11**, 2191.
6 J. Wen, Y. Yu and C. Chen, *Mater. Express*, 2012, **2**, 197.
7 X. Su, F. Dogan, J. Ilavsky, V. A. Maroni, D. J. Gosztola and W. Lu, *Chem. Mater.*, 2017, **29**, 6205.
8 D. Liu, Z. Shadike, R. Lin, K. Qian, H. Li, K. Li, S. Wang, Q. Yu, M. Liu, S. Ganapathy, X. Qin, Q.-H. Yang, M. Wagemaker, F. Kang, X.-Q. Yang and B. Li, *Adv. Mater.*, 2019, **31**, 1806620.
9 Y. Ma, S. Li and B. Wei, *Nanoscale*, 2019, **11**, 20429.
10 J. R. Rodriguez, S. B. Aguirre and V. G. Pol, *Electrochim. Acta*, 2019, **319**, 791.
11 F. Blanc, M. Leskes and C. P. Grey, *Acc. Chem. Res.*, 2013, **46**, 1952.
12 M. Letellier, E*ncycl. Spectrosc. Spectrom.*, 2017, **2**, 181.
13 F. Chevallier, M. Letellier, M. Morcrette, J. M. Tarascon, E. Frackowiak, J. N. Rouzaud and F. Beguin, *Electrochem. Solid-State Lett.*, 2003, **6**, A225.
14 M. Letellier, F. Chevallier, C. Clinard, E. Frackowiak, J.N. Rouzaud, F. Beguin, M. Morcrette and J.M. Tarascon, *J. Chem. Phys.*, 2003, **118**, 6038.
15 M. Letellier, F. Chevallier, F. Beguin, E. Frackowiak and J.N. Rouzaud, *J. Phys. Chem. Solids*, 2004, **65**, 245.
16 M. Letellier, F. Chevallier and F. Beguin, *J. Phys. Chem. Solids*, 2006, **67**, 1228.

17 M. Letellier, F. Chevallier and M. Morcrette, *Carbon*, 2007, **45**, 1025.
18 F. Chevallier, F. Poli, B. Montigny and M. Letellier, *Carbon*, 2013, **61**, 140.
19 K. Gotoh, M. Izuka, J. Arai, Y. Okada, T. Sugiyama, K. Takeda and H. Ishida, *Carbon*, 2014, **79**, 380.
20 J. Arai, Y. Okada, T. Sugiyama, M. Izuka, K. Gotoh and K. Takeda, *J. Electrochem. Soc.*, 2015, **162**, A952.
21 J.M. Stratford, P.K. Allan, O. Pecher, P.A. Chater and C.P. Grey, *Chem. Commun.*, 2016, **52**, 12430.
22 K. Ogata, E. Salager, C.J. Kerr, A.E. Fraser, C. Ducati, A.J. Morris, S. Hofmann and C.P. Grey, *Nature Commun.*, 2014, **5**, 4217.
23 P.K. Allan, J.M. Griffin, A. Darwiche, O.J. Borkiewicz, K.M. Wiaderek, K.W. Chapman, A.J. Morris, P.J. Chupas, L. Monconduit and C.P. Grey, *J. Am. Chem. Soc.*, 2016, **138**, 2352.
24 X. Feng, M. Tang, S. O'Neill and Y.-Y. Hu, *J. Mater. Chem. A*, 2018, **6**, 22240.
25 A.I. Freytag, A.D. Pauric, M. Jiang and G.R. Goward, *J. Phys. Chem. C*, 2019, **123**, 11362.
26 V. Küpers, M. Kolek, P. Bieker, M. Winter and G. Brunklaus, *Phys. Chem. Chem. Phys.*, 2019, **21**, 26084.
27 J.L. Lorie Lopez, P.J. Grandinetti and A.C. Co, *J. Mater. Chem. A*, 2019, **7**, 10781.
28 K. Kitada, O. Pecher, P.C.M.M. Magusin, M.F. Groh, R.S. Weatherup and C.P. Grey, *J. Am. Chem. Soc.*, 2019, **141**, 7014.
29 A. I. Freytag, A. D. Pauric, S. A. Krachkovskiy and G. R. Goward, *J. Am. Chem. Soc.*, 2019, **141**, 13758.
30 J. Arai, K. Gotoh, R. Sayama and K. Takeda, *J. Electrochem. Soc.*, 2017, **164**, A6334.
31 K. Gotoh, M. Maeda, A. Nagai, A. Goto, M. Tansho, K. Hashi, T. Shimizu and H. Ishida, *J. Power Sources*, 2006, **162**, 1322.
32 R. Morita, K. Gotoh, K. Kubota, S. Komaba, K. Hashi, T. Shimizu and H. Ishida, *Carbon*, 2019, **145**, 712.
33 N.M. Trease, L. Zhou, H. J. Chang, B.Y. Zhu and C.P. Grey, *Solid State Nuc. Mag. Res.*, 2012, **42**, 62.
34 R. Bhattacharyya, B. Key, H. Chen, A.S. Best, A.F. Hollenkamp and C.P. Grey, *Nature Mater.*, 2010, **9**, 504.
35 S. Chandrashekar, N.M. Trease, H.J. Chang, L.-S. Du, C.P. Grey and A. Jerschow, *Nature Mater.*, 2012, **11**, 311.
36 R. Morita, K. Gotoh, M. Fukunishi, K. Kubota, S. Komaba, N. Nishimura, T. Yumura, K. Deguchi, S. Ohki, T. Shimizu and H. Ishida, *J. Mater. Chem. A*, 2016, **4**, 13183.